High-Power Large-Aperture Bottom-Emitting 980-nm VCSELs With Integrated GaAs Microlens

Zhenfu Wang, Yongqiang Ning, Te Li, Jinjiang Cui, Yan Zhang, Guangyu Liu, Xing Zhang, Li Qin, Yun Liu, and Lijun Wang

***Abstract*—Microlens-integrated bottom-emitting 980-nm vertical-cavity surface-emitting lasers (VCSELs) with an emitting window aperture of 400 μm have been fabricated. A novel material structure with nine InGaAs–GaAsP quantum wells and slightly decreased reflectivity of n-type distributed Bragg reflectors (n-DBRs) are employed to increase the output power. A convex microlens is fabricated by a one-step diffusion-limited wet-etching technique on the GaAs substrate. The diameter of the active layer is about 200 μm after lateral oxidation, and the nominal diameter of the microlens is 400 μm. The maximum output power is 200 mW at continuous-wave operation at room temperature. The far-field divergence angles $\theta_{\|}$ and $\theta_{\perp}$ of the single device at a current of 4A are 8.7° and 8.4°, respectively. The optical beam performance between the microlens-integrated VCSEL and ordinary VCSEL is compared.**

***Index Terms*—Full-width at half-maximum (FWHM), microlens, power, vertical-cavity surface-emitting lasers (VCSELs).**

I. Introduction

The vertical-cavity surface-emitting laser (VCSEL) has been proven to be a low-cost light source with attractive properties such as low threshold current, wafer-level testing, compatibility with flip-chip bonding, and easy fabrication of two-dimensional arrays. These features, together with its high-speed modulation, have made it a widespread application in, for example, short-distance parallel fiber-optic interconnects. The output power of a single device is reported to be above 3 W [1]. However, the beam quality of the large diameter device is deteriorated due to the inhomogeneous current distribution across the active region. Collimating optical elements are often required to improve the beam quality. A microlens could be fabricated directly onto the surface of the emitting window to present an additional optical feedback, which could stabilize the fundamental transverse mode operation. More particularly, the integration of GaAs microlens directly on the substrate of the VCSEL can offer large alignment tolerance, accompanied with the advantages of simple and compact device packaging.

Up to now, various fabrication techniques for monolithic microlens-integrated VCSELs, such as photoresist reflow followed by dry-etching [2], focused ion beam milling [3], mass transport after preshaping [4], and shadow mask regrowth [5] have been reported. Yet, those methods require multiple process steps or expensive processing equipment, which are not generally compatible with cost-effective commercial production requirements. In order to obtain the high power and good beam quality, a larger aperture microlens-integrated VCSEL is fabricated by a one-step diffusion-limited wet-etching process taking the cost-effective requirement into account [6].

Manuscript received October 16, 2008; revised November 19, 2008. First published January 06, 2009; current version published February 04, 2009. This work is supported by the National Natural Science Foundation of China under Grant No. 60636020, 60676034, 60476029, 60577003, 60876036 and 60706007.

The authors are with the Key Laboratory of Excited State Processes, Changchun Institute of Optics, Fine Mechanics and Physics, Chinese Academy of Sciences, Changchun 130033, China (e-mail: ningyq@ciomp.ac.cn).

Digital Object Identifier 10.1109/LPT.2008.2010510

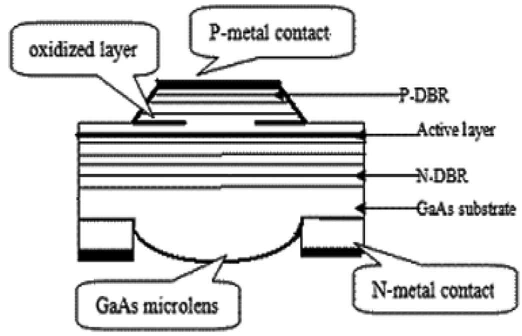

Fig. 1. Schematic diagram of microlens-integrated 980-nm bottom-emitting oxide-confined VCSEL.

II. Structure and Fabrication of Microlens-Integrated VCSEL

The structure of the microlens-integrated 980-nm bottom-emitting oxide-confined VCSEL is schematically illustrated in Fig. 1. The conventional 980-nm VCSEL structure is composed of three InGaAs–GaAs quantum wells. In this letter, a novel material structure with nine InGaAs–GaAsP quantum wells periodically distributed into three groups inside the cavity and slightly decreased reflectivity of an n-type distributed Bragg reflector (n-DBR) is employed to increase the output power. The total structure has a two-λ-thick Al_xGa_{1-x} As microcavity spacer with nine $In_{0.2}Ga_{0.8}As$ (6 nm)/$Ga_{0.18}As_{0.82}P$ (8 nm) quantum wells embedded in the antinodes of the cavity. GaAsP barrier with a slightly wider bandgap than GaAs is used to increase the carrier confinement in the quantum well and therefore improve the operation performance at elevated temperature. The p-Bragg stack is built of 30 pairs of quarter-wavelength-thick $Al_xGa_{1-x}As$–GaAs with a graded interface providing 99.9% reflectivity. To reduce the series resistance of p-DBR, carbon is employed as a p-type dopant. In order to decrease the voltage drop without increasing absorption losses, an extra modulated doping near interface is necessary. When a 30-nm-thick AlAs layer located above the p-type cladding layer is oxidized and converted into Al_xO_y layer, which can supply lateral confinement to the current and light in the device. The n-type Si-doped Bragg stack is composed of 25 pairs of $Al_xGa_{1-x}As$ providing 99.3% reflectivity. Compared to the conventional 28 pairs of $Al_xGa_{1-x}As$, the decreased reflectivity of n-DBR is beneficial

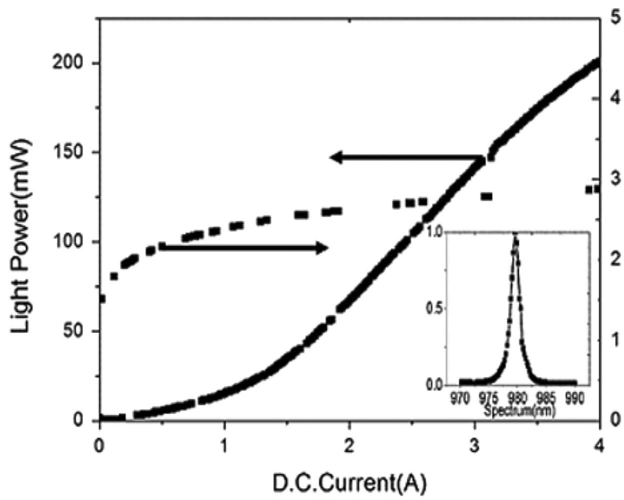

Fig. 2. L–I, V–I, and spectrum characteristics of microlens-integrated VCSEL.

for high output power with a compromise of slightly increased threshold current.

Wet chemical etching is used to form a circular mesa with an etching depth down to AlAs layer for lateral oxidization. The AlAs layer is oxidized about 60 min at 420 °C under nitrogen gas bubbled through water at 90° to form current apertures with oxidation depths from 20 to 30 μm. The surface is passivated with Al_2O_3 and a circular window on the top of the mesa is opened for evaporating a full size Ti–Au–Pt–Au P-type contact to provide a homogeneous current distribution and serve as a metal pad for soldering.

Then, a 100-nm-thick SiO_2 masking layer was deposited on GaAs substrate, whereafter, circular holes with an appropriate diameter are formed on the SiO_2 masking layer by standard photolithography to expose the emitting window. The patterned samples are immersed in a diffusion-limited etchant, which is composed of HBr, H_2O_2, and H_2O. Due to the low mobility of Br_2 molecular, Br_2 molecular near the edge of circular hole is consumed much faster than in the center of circular hole. Such the spatial variation in the etching rate across the emitting window forms a spherical profile on the surface of the substrate. The lens curvature radius is dependent on the etching time and the composition ratio of the solution. Moreover, the etching progress should set in the static environment because any disturbance against the nature diffusive motion of the etching species would alter the details of microlens. The atomic force microscope (AFM) technique is employed to quantitatively evaluate the surface profile of microlens. The curvature radius of microlens of 959.75 μm and the focal length of 369.13 μm is achieved. The root-mean-square (rms) of the whole microlens surface is about 14.15 nm.

III. Result and Discussion

The light output–current (L–I), voltage–current (V–I) characteristics of a microlens-integrated VCSEL single device are shown in Fig. 2. The threshold current, threshold voltage, and differential resistance of the device are 1.09 A, 2.19 V, and 0.1 Ω, respectively. A maximum output power under continuous-wave (CW) operation is 200 mW at room temperature due to the limits of thermal rollover, which is the highest value reported for a microlens-integrated VCSEL [7]. The maximum slop efficiency is 0.07 W/A, which is greatly lower due to much more internal heating in the active region and the larger scattering losses of the microlens surface. The inset shows the lasing spectrum measured at a current of 4 A. The peak wavelength is 978.1 nm with a full-width at half-maximum (FWHM) of 0.8 nm. The far-field FWHM divergence angle $\theta_{||}$ (lateral divergence angle) and $\theta_{\perp}$ (vertical divergence angle) are 8.7°, 8.4°, respectively, as demonstrated in Fig. 3(a).

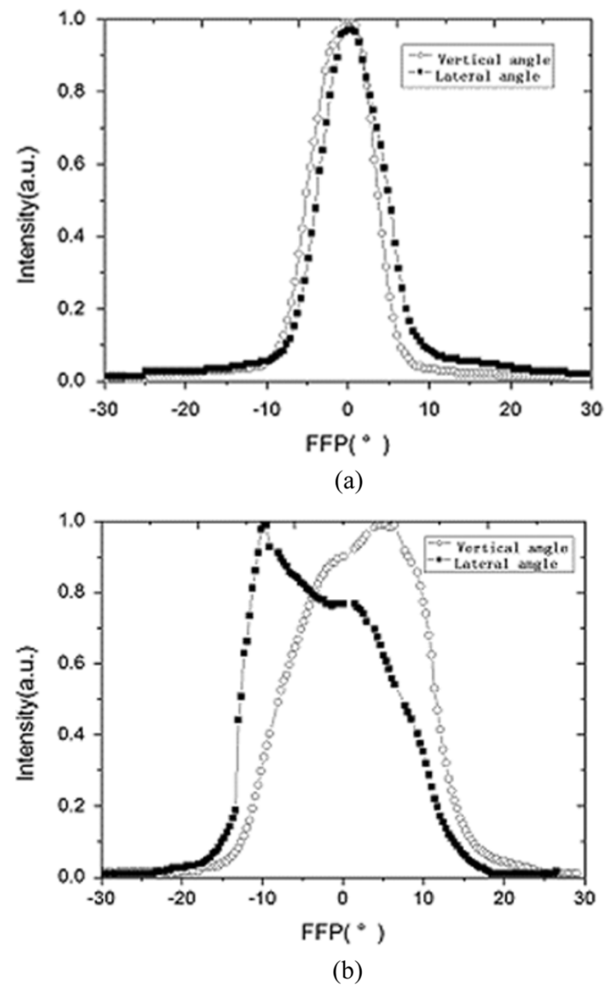

Fig. 3. Comparison of far-field distribution of microlens-integrated and conventional VCSEL at a current of 4 A. (a) Microlens-integrated VCSEL. (b) Conventional VCSEL without microlens.

The operation characteristics between microlens-integrated VCSEL and conventional VCSEL without microlens have also been investigated. Due to the microlens on GaAs substrate, the equivalent reflectivity $R'_{\rm bot}$ of n-DBR should be slightly increased. However, because of the microlens-integration on n^+-GaAs substrate, the effective cavity length is elongated, and the relatively larger roughness of the microlens surface creates additional scattering losses. It can be concluded that the threshold current of microlens-integrated VCSEL (1.09 A) could be a little bit higher than that of conventional VCSEL (0.93 A) from the following empirical formula:

$$I_{\rm th} = \frac{eMV_a}{\eta_i \tau_{\rm sp}} N_{\rm tr} \exp\left\{ \frac{1}{ML_z} \left[L_{\rm eff}\alpha_i + \frac{1}{2}\ln\left(\frac{1}{R_{\rm top}R'_{\rm bot}}\right)\right]\right\}$$

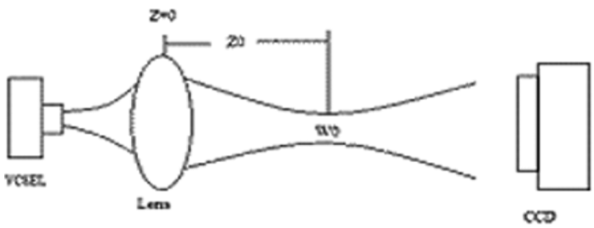

Fig. 4. Schematic measurement setup for the M^2 factor.

where e, M, $V_a, \eta_i, \tau_{\rm sp}$, $\mathrm{N_{tr}}$, L_z, $L_{\rm eff}, \alpha_i$, $R_{\rm top}$, and $R'_{\rm bot}$ are the charge of electron, the number of quantum wells, the volume of the active region, the internal quantum efficiency, the carrier lifetime, the transparent carrier density, the width of quantum well, the effective cavity length, the total loss of scattering and absorption, the reflectivity of p-DBR, and the equivalent reflectivity of n-DBR, and microlens.

The obvious improvement is the far-field divergence angle of 8.7° and 8.4° at the two directions compared to the much higher divergence angle of 18.9° and 19.8° for conventional VCSEL device at a current of 4 A, as shown in Fig. 3(a) and (b). The convex GaAs-microlens can introduce a small additional reflectivity when the light travels through the microlens, so the light emitted out of the n-DBR is partly reflected by the surface of the convex microlens back into the active region. The fed-back light overlaps in the quantum-well active layer. The total accumulative field strength that the quantum-well active layer experiences is, therefore, spatially concentrated toward the aperture center, which can effectively stabilize the laser mode to realize fundamental transverse-mode operation [8].

The beam quality factors (M^2 factor) between the microlens-integrated VCSEL and conventional VCSEL with the same emitting window aperture of 400 μm have also been investigated. The product of beam waist and divergence angle for an ideal Gaussian beam is described by

$$\omega_0 \bullet \theta = \frac{\lambda}{\pi}$$

where ω_0 is the radius of the beam waist, θ is the divergence angle. However, to describe a real laser beam, M^2 factor should be included in the product of beam waist and divergence angle just as

$$W_0 \bullet \Theta = \frac{\lambda}{\pi} M^2$$

where W_0 is the radius of the real laser beam, Θ is the divergence angle of the real laser beam.

The measurement setup for the M^2 factor is schematically illustrated in Fig. 4. The laser beam of the microlens-integrated VCSEL travels through a lens to form a beam waist at a distance of Z_0. The position of lens is set to be 0. The beam width W is calculated from a series of pictures at different positions along the Z-axis captured by a charged-coupled device camera. The values of M^2 factor and the beam waist W_0 can be calculated by

$$M^2 = \frac{\pi W_0^2}{\lambda (Z - Z_0)} \sqrt{\frac{W^2(Z) - W_0^2}{W_0^2}}$$

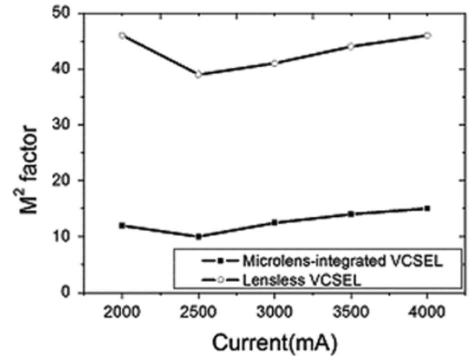

Fig. 5. M^2 factors of the microlens-integrated and conventional VCSEL at different currents.

where λ is the emitting wavelength. The M^2 factor of the microlens-integrated VCSEL is much smaller than that of a conventional VCSEL at the same operating current [9], as illustrated in Fig. 5. It is also found that the beam qualities of both kinds of lasers will be deteriorated as increasing the operating current, which is caused by the current crowding due to the ring shape of n-contact.

IV. Conclusion

Microlens-integrated bottom-emitting 980-nm VCSELs with an output aperture of 400 μm are fabricated with a diffusion-limited wet-etching technique. The maximum CW output power of 200 mW is achieved at room temperature. The peak wavelength is 978.1 nm and the FWHM of the spectrum is 0.8 nm. The microlens-integrated VCSEL improves greatly the far-field distribution profile with much smaller divergence angles of 8.7° and 8.4°, and the beam quality factor of it is around 10.

References

[1] L. A. D'Asaro, J.-F. Seurin, and J. D. Wynn, "High-power, high efficiency VCSELs pursue the goal," *Photon. Spectra*, vol. 2, pp. 64–66, 2005.

[2] E. M. Strzelecka, G. D. Robinson, L. A. Coldren, and E. L. Hu, "Fabrication of refractive microlenses in semiconductors by mask shape transfer in reactive ion etching," *Microelectron. Eng.*, vol. 35, pp. 385–388, 1997.

[3] Y. Fu, "Integration of micro diffractive lens with continuous relief with vertical-cavity surface-emitting lasers using focused ion beam direct milling," *IEEE Photon. Technol. Lett.*, vol. 13, no. 5, pp. 424–426, May 2001.

[4] Z. L. Liau, D. E. Mull, C. L. Dennis, and R. C. Williamson, "Large-numerical-aperture microlens fabrication by one-step etching and mass-transport smoothing.," *Appl. Phys. Lett.*, vol. 64, pp. 1484–1486, Mar. 1994.

[5] G. M. Peake, S. Z. Sun, S. D. Hersee, and J. Electron, "GaAs microlens arrays grown by shadow masked MOVPE.," *J. Electron. Mater.*, vol. 26, pp. 1134–1138, Oct. 1997.

[6] Y. Fu and N. K. Bryan, "Semiconductor microlenses fabricated by one-step focused ion beam direct writing.," *IEEE. Photon. Technol. Lett.*, vol. 15, no. 5, pp. 229–231, May 2002.

[7] S.-H. Park, S. Lee, and H. Jeon, "Mode-stabilized operation in a microlens-integrated 980 nm vertical-cavity surface-emitting laser," *Opt. Rev.*, vol. 13, pp. 146–148, Mar. 2006.

[8] S.-H. Park, Y. Park, and H. Jeon, "Theory of the mode stabilization mechanism in concave-micro mirror-capped vertical-cavity surface-emitting lasers," *J. Appl. Phys.*, vol. 94, pp. 1312–1317, Aug. 2003.

[9] L. Te *et al.*, "Beam quality of 980 nm high power vertical-cavity surface-emitting lasers," *Chin. J. Lasers*, vol. 34, pp. 641–645, May 2007.